Editors' Suggestion

Clustering and energy spectra in two-dimensional dusty gas turbulence

Vikash Pandey* and Prasad Perlekar†
TIFR Centre for Interdisciplinary Sciences, Hyderabad 500107, India

Dhrubaditya Mitra‡
NORDITA, Royal Institute of Technology and Stockholm University, SE-10691 Stockholm, Sweden

(Received 18 February 2019; published 26 July 2019)

We present direct numerical simulation of heavy inertial particles (dust) immersed in two-dimensional turbulent flow (gas). The dust particles are modeled as monodispersed heavy particles capable of modifying the flow through two-way coupling. By varying the Stokes number (St) and the mass-loading parameter (ϕ_m), we study the clustering phenomenon and the gas phase kinetic energy spectra. We find that the dust-dust correlation dimension (d_2) also depends on ϕ_m. In particular, clustering decreases as mass loading (ϕ_m) is increased. In the kinetic energy spectra of gas we show (i) the emergence of a different scaling regime and that (ii) the scaling exponent in this regime is not universal but a function of both St and ϕ_m. Using a scale-by-scale enstrophy budget analysis we show that in this emerged scaling regime, which we call the dust-dissipative range, viscous dissipation due to the gas balances the back-reaction from the dust.

DOI: 10.1103/PhysRevE.100.013114

I. INTRODUCTION

In nature, turbulent flows often include small particles embedded within the flow; typical examples are (a) protoplanetary disks (gas and dust) [1], (b) clouds (air and water droplets) [2], and (c) aeolian processes (wind and sand) [3]. Analytical, numerical, and experimental studies of such multiphase flows have flourished in the last decade (see, e.g., Refs. [4–7] for a review). For notational convenience, in the rest of this paper, we call the solvent phase "gas" and the solute phase "dust." Often the simplest model used to study such multiphase flows assumes that the dust is a collection of heavy, inertial particles (HIPs) which do not alter the gas flow. The equations of motion of the dust particles are as follows:

$$\frac{d\boldsymbol{X}(t)}{dt} = \boldsymbol{V}(t), \tag{1a}$$

$$\frac{d\boldsymbol{V}(t)}{dt} = \frac{1}{\tau_p}[\boldsymbol{u}(\boldsymbol{X},t) - \boldsymbol{V}], \tag{1b}$$

where $\boldsymbol{X}$ is the position, $\boldsymbol{V}$ is the velocity of a dust particle, $\boldsymbol{u}$ is the velocity of the gas at a point $\boldsymbol{X}$, and $\tau_p \equiv 2\rho_d a^2/9\rho_g\nu$ is the particle relaxation time. Here a is the particle radius, ν is the kinematic viscosity of the gas, and ρ_g (ρ_d) is the gas (particle) density. For incompressible flows, in addition to the Reynolds number, an additional dimensionless number appears, the Stokes number $\mathrm{St} \equiv \tau_p/\tau_\eta$, where τ_η is a characteristic timescale of the flow of gas. If the size of dust grains are comparable to or larger than the dissipative scales of the flow, then the simple approximation encoded in Eq. (1) is not valid anymore. Furthermore, Eq. (1) is a reasonable model of reality if the number density of the dust grains is so small that both the dust-dust interaction and the back-reaction from the dust phase to the gas phase can be ignored. In this paper, we study the consequences of relaxing this last assumption. One of our motivations is the recent realization that the dust in astrophysical plasma cannot be treated merely as a passive component. In particular, the inclusion of the back-reaction allows for novel instabilities, e.g., the streaming instability [8,9], to manifest themselves.

In the absence of dust, the turbulence in the gas phase has been extensively studied [10–12]. The pioneering work of Kolmogorov [13] has established that in three dimensions the (angle-integrated) energy spectrum of the gas shows the power-law behavior $E(k) \sim k^{-5/3}$ within the inertial range followed by the dissipation range where the energy spectrum shows exponential decay [14]. More importantly, the inertial range spectral exponent is universal; i.e., it does not depend on the Reynolds number and the mechanism of turbulence generation. Does the presence of dust modify this energy spectrum? Obviously, in general, the answer depends on the number, size, and shape of the dust grains. In this paper, we study this question using direct numerical simulations (DNS) of the dusty gas flow.

A recent paper [15] has suggested that in the presence of dust a power-law behavior can emerge where $E(k) \sim k^{-4}$ in three dimensions. Is this exponent universal, in the sense that, is it independent of the Stokes number and the dust concentration? It is difficult to provide an answer to this question because an accurate determination of the exponent requires obtaining clean scaling of the energy spectrum over at least a decade. This is a formidable task in three dimensions but is a much simpler proposition in two dimensions. Hence to understand the universality (or lack thereof) we study this problem in two dimensions.

Two-dimensional turbulence is the simplest model to investigate flows in the atmosphere and oceans [10,12,16]. A

*vikashpandey.phy@gmail.com
†perlekar@tifrh.res.in
‡dhruba.mitra@gmail.com

key feature of two-dimensional turbulence is that it supports a bidirectional cascade, an inverse cascade of energy from forcing scales to larger scales and a forward enstrophy cascade from forcing scales to smaller scales [17–22]. As we are interested in investigating how dust modifies small-scale flow properties, we concentrate on the forward enstrophy cascade.

In two-dimensional gas turbulence, forced at large scales (small k) and in the presence of air-drag friction (α), the scaling exponent of the energy spectrum is universal with respect to the Reynolds number but *nonuniversal* in general—it depends on the air-drag-friction coefficient [23,24]. The scaling exponent and its nonuniversality can be understood as an effect of the loss of enstrophy due to air-drag friction [25]. In our simulations, we choose an α such that in the absence of dust $E(k) \sim k^{-3.9}$. We then perform extensive simulations of the dusty-gas flow by varying both the Stokes number and the mass-loading parameter ($\phi_{\rm m}$, ratio of the total mass of the dust to the total fluid mass).

The rest of the paper is organized in the following manner. In Sec. II we present our model and describe how it is implemented numerically. Under Results, Sec. III A is devoted to the discussion of the pair-distribution function of dust particles where we show that increasing the mass-loading parameter reduces the clustering of dust. In Secs. III B and III C, we present energy spectra and a scale-by-scale enstrophy budget, respectively, for the gas phase. We show that indeed in the presence of dust-gas coupling, a different scaling range, which we call the dust-dissipative range, emerges in the kinetic energy spectra of the gas. Furthermore, using a scale-by-scale enstrophy budget analysis we show that the scaling regime appears due to a balance between the injection (from the dust to the gas) and viscous dissipation. Our main result is that the scaling exponent is *not universal* but depends on both the St and the mass-loading parameter $\phi_{\rm m}$. Finally, in Sec. IV we conclude the paper.

II. MODEL AND NUMERICAL METHOD

The dust is modeled as a system of monodispersed spherical particles governed by Eq. (1). Gas is modeled in the Eulerian framework where the equation for the scalar vorticity field $\omega(\boldsymbol{x},t) \equiv \boldsymbol{\nabla} \times \boldsymbol{u}(\boldsymbol{x},t)$ is

$$D_t\omega(\boldsymbol{x},t) = \nu\nabla^2\omega(\boldsymbol{x},t) - \alpha\omega(\boldsymbol{x},t) + f(\boldsymbol{x},t) + \boldsymbol{\nabla} \times \boldsymbol{F}^{\rm d\to g}(\boldsymbol{x},t). \quad (2)$$

Here $\boldsymbol{u}(\boldsymbol{x},t)$ is the incompressible velocity field, $D_t = \partial_t + \boldsymbol{u}\cdot\boldsymbol{\nabla}$ is the material derivative, ν is the viscosity, α is the Ekman drag coefficient, and $f(\boldsymbol{x},t) = -f_0 k_{\rm f}\cos(k_{\rm f}y)$ is the Kolmogorov forcing with amplitude f_0 and at wave number $k_{\rm f}$. The force exerted by the dust particles on the gas is

$$\boldsymbol{F}^{\rm d\to g}(\boldsymbol{x},t) = \sum_{i=1}^{N_{\rm p}} \frac{m}{\tau_{\rm p}\rho_{\rm g}}[\boldsymbol{V}_i - \boldsymbol{u}(\boldsymbol{x},t)]\delta^2(\boldsymbol{x}-\boldsymbol{X}_i), \quad (3)$$

where m is the mass of a dust particle, and $N_{\rm p}$ is the total number of particles. We use a pseudospectral method [26,27] with 2/3 dealiasing to numerically integrate Eq. (2) in a periodic square box with each side of length $L = 2\pi$. The simulation domain is spatially discretized using N^2 collocation points. Thus the maximum resolved wave number after deasliasing is $k_{\rm max} = N/3$. For time evolution we employ a second-order Runge-Kutta scheme [28]. Once a statistically stationary state is obtained, we continue the DNS for another $35\tau_{\rm L}$, where $\tau_{\rm L} \equiv 2\pi/k_{\rm f}u_{\rm rms}$ is the large-eddy-turnover time, to collect statistics of the turbulent flow. The Kolmogorov timescale $\tau_\eta \equiv \sqrt{\nu/\epsilon}$, where ϵ is the energy dissipation rate, is approximately $\tau_{\rm L}/6$ in our simulation.

In this Eulerian-Lagrangian framework, the position of a dust grain does not, in general, coincide with the Eulerian grids. The gas velocity at the position of a dust particle in Eq. (1b) is obtained as

$$\boldsymbol{u}(\boldsymbol{X},t) = \sum_{\boldsymbol{x}} \boldsymbol{u}(\boldsymbol{x},t)\delta_{\rm h}^2(\boldsymbol{x}-\boldsymbol{X})h^2, \quad (4)$$

where $h = L/N$, and $\delta_h^2(\cdot)$ is a numerical realization of the two-dimensional δ function on grids of linear dimension h. We use the following prescription [29]:

$$\delta(x-X) = \begin{cases} \frac{1}{4h}\left\{1+\cos\left[\frac{\pi(x-X)}{2h}\right]\right\}, & |x-X| \leqslant 2h, \\ 0 & \text{otherwise.} \end{cases} \quad (5)$$

The same prescription, Eq. (5), is also used to discretize the δ function in Eq. (3). We initialize our simulation with $N_{\rm p}$ randomly placed dust particles. Similar to aerosols in clouds [30], we assume that the ratio of the material density of dust over the gas density is $\rho_{\rm d}/\rho_{\rm g} \sim 10^3$. The vorticity is initialized as $\omega(\boldsymbol{x},0) = -f_0 k_{\rm f}\nu[\cos(k_{\rm f}x) + \cos(k_{\rm f}y)]$.

III. RESULTS

We study the dust-gas turbulence by varying the mass-loading parameter $\phi_{\rm m} \equiv N_{\rm p}m/(\rho_{\rm g}L^2)$ and the Stokes number St.

A. Vorticity and clustering

In Fig. 1 we show a representative pseudocolor plot of the vorticity field in the absence of dust ($\phi_{\rm m} = 0$) and at high mass-loading $\phi_{\rm m} = 1$. We observe that in the latter case small-scale vortices form in the regions where dust particles cluster. Our observation is consistent with the earlier study of two-dimensional dusty-gas turbulence [31]. We quantify the clustering by using the cumulative pair distribution function

$$N(r) \equiv \left\langle \frac{2}{N_{\rm p}(N_{\rm p}-1)} \sum_{i<j} \Theta(r - |\,\mathbf{X}_i - \mathbf{X}_j\,|) \right\rangle. \quad (6)$$

Here Θ is the Heaviside function and the angular brackets denote averaging over different stationary-state turbulent configurations. In Fig. 2(a), we plot $N(r)$ versus r for fixed $\phi_{\rm m} = 1$ and with different St. In the limit $r \to 0$, $N(r) \sim r^{d_2}$, where d_2 is the correlation dimension [32]. We obtain d_2 by performing a least-square fit in the range $1 < r\eta < 10$.

In Fig. 2(b) we plot the correlation dimension d_2 as a function of St for different values of $\phi_{\rm m}$. Note that $d_2 = 2$ for St $= 0$ and ∞ and attains a minimum value, which corresponds to maximum clustering, around St ≈ 0.6 [33]. We observe that for all the values of $\phi_{\rm m}$ this is indeed the case. However, the amount of clustering (d_2) decreases (increases) with increasing $\phi_{\rm m}$. We find that for a fixed St, the maximum clustering is obtained for one-way coupled simulations where

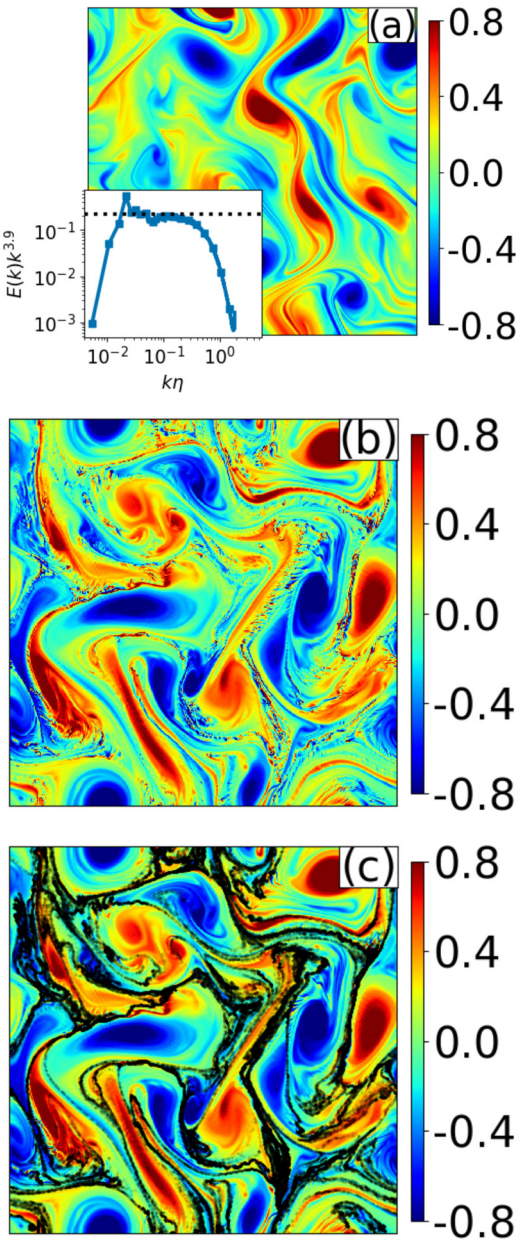

FIG. 1. (a) Representative steady-state snapshot of the vorticity field (ω) from our simulation for $\phi_m = 0$. (Inset) Log-log plot of the compensated energy spectrum $[k^{3.9}E(k)]$ versus $k\eta$, where η is the Kolmogorov dissipation length scale. (b) Representative snapshot of ω during the steady state for St $= 0.33$ and $\phi_m = 1.0$. (c) The positions of all the dust particles are overlaid as black dots on the underlying vorticity plot of panel (b). The diameter of each dust particle is assumed to be much smaller than η. We use the following parameters: $\alpha = 10^{-2}$, $f_0 = 5 \times 10^{-3}$, $k_f = 4$, and $\nu = 10^{-5}$; $N = 1024$ for all the simulations in Sec. III A and $N = 4096$ for simulations in Secs. III B and III C. For $\phi_m = 0$, we find the Kolmogorov dissipation length $\eta[\equiv (\nu^3/\epsilon)^{1/4}] = 5.4 \times 10^{-3}$, the Kolmogorov dissipation time scale $\tau_\eta(\equiv \sqrt{\nu/\epsilon}) = 2.9$, and enstrophy dissipation rate $\beta = 2.8 \times 10^{-4}$. We vary St in the range 0.17–1.67 and N_p in the range 1.5×10^4–1.5×10^5 to achieve mass loading (ϕ_m) of 0.1–1.0, respectively. The only exception is made for St $= 0.17$ in Secs. III B and III C, where we take $N_p = 4.5 \times 10^5$ to achieve $\phi_m = 1$.

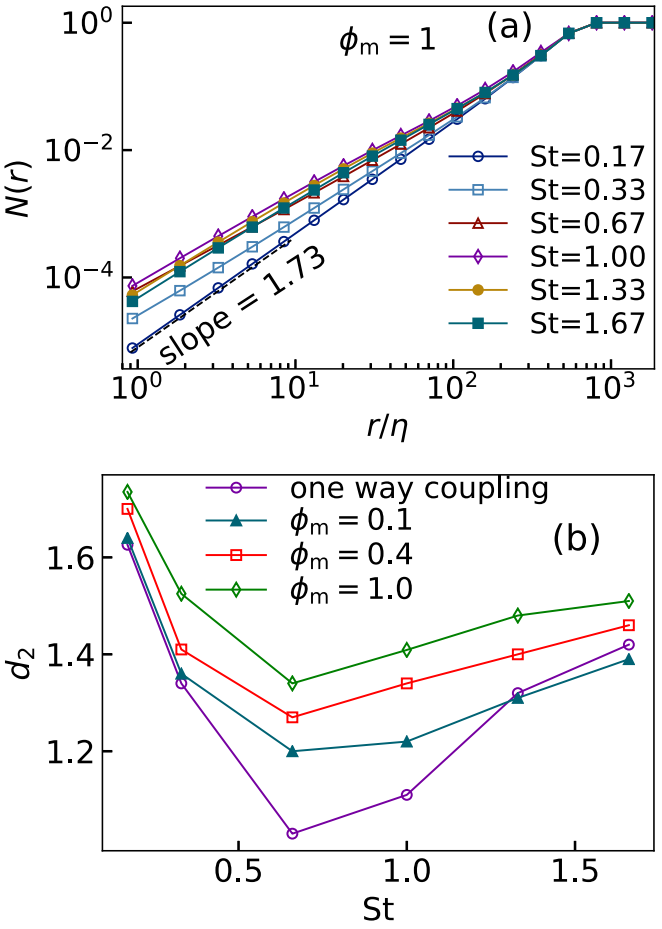

FIG. 2. (a) Log-log plot of the cumulative distribution function $N(r)$ vs r/η for $\phi_m = 1$ and different St. The dashed line represents the least-square fit with the corresponding value of the slope. (b) The correlation dimension d_2 vs St for different ϕ_m.

the back-reaction from the dust is ignored. Similar results have also been observed for particle-laden turbulent homogeneous shear flows [15,34]. Qualitatively, the small-scale vortices produced in the presence of mass loading expel particles; hence clustering reduces as ϕ_m increases.

B. Energy spectra

Next, we study the angle-averaged velocity power spectrum,

$$E(k) \equiv \frac{1}{2}\left\langle \sum_{k-1/2 \leqslant |\boldsymbol{m}| < k+1/2} |\, \boldsymbol{u_m}\,|^2 \right\rangle, \tag{7}$$

where $\boldsymbol{u_m}$ is the velocity at the Fourier mode $\boldsymbol{m}$. In the absence of dust particles ($\phi_m = 0$), the energy spectrum [Fig. 1(a)] shows inertial range scaling $E(k) \sim k^{-3.9}$ for $0.03 \leqslant k\eta \leqslant 0.1$ and decays exponentially in the dissipation range ($k\eta > 0.10$) [27].

We find that, once the feedback from the dust phase to the gas phase is included, the energy spectra changes dramatically in the following manner: the inertial range scaling with an exponent of $k^{-3.9}$ persists till a critical wave number k_c; for $k > k_c$, we observe a different power law $E(k) \sim k^{-\xi}$,

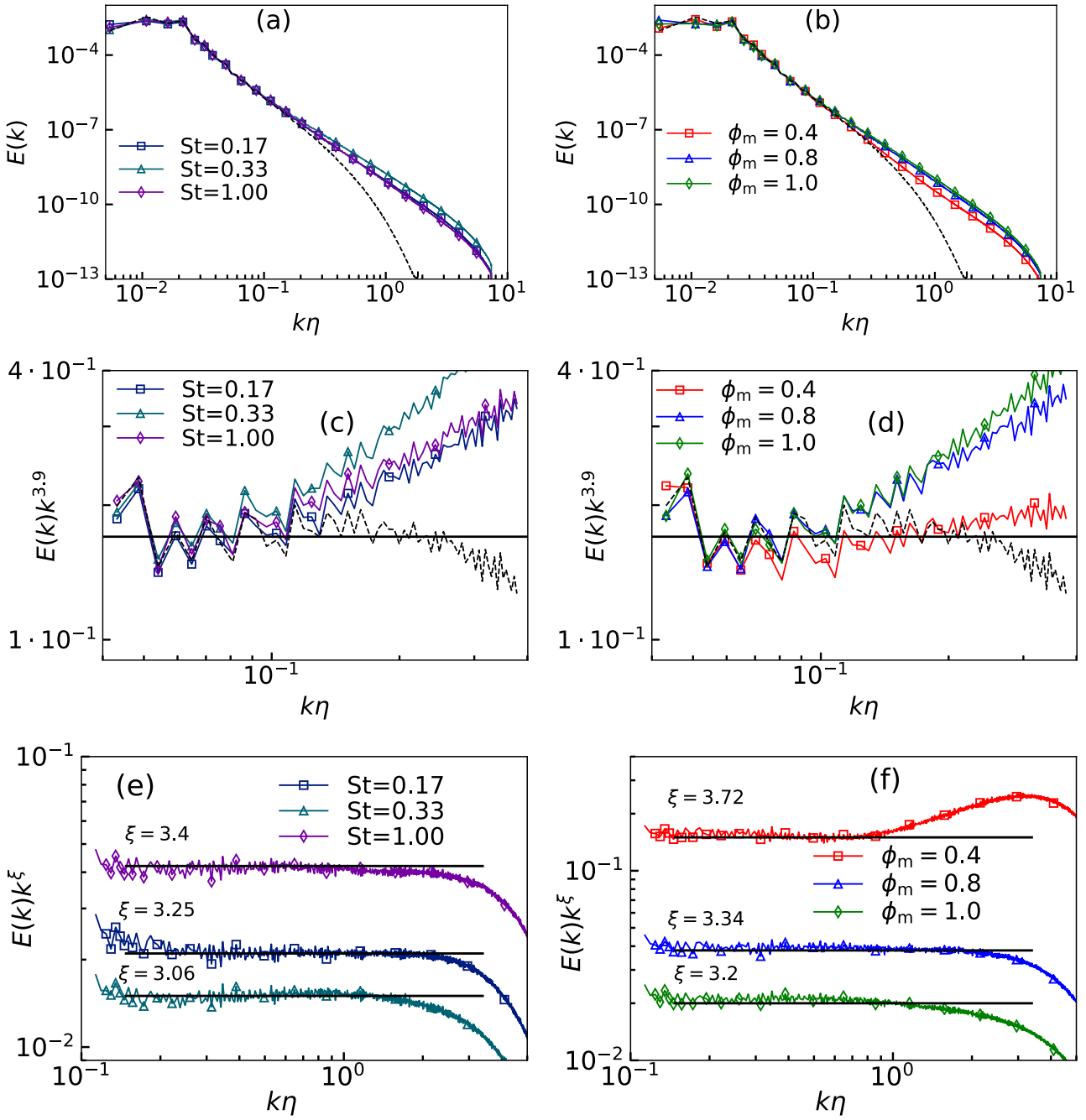

FIG. 3. Log-log plot of energy spectra for (a) $\phi_m = 1.0$, different values of St, and (b) St = 0.67, different values of ϕ_m. The black dashed lines show $E(k)$ for $\phi_m = 0$. (c, d) Log-log plot of energy spectra $E(k)$ compensated by $k^{3.9}$. The black dashed lines show the compensated spectra for the case $\phi_m = 0$, i.e., no feedback. Once the feedback is included, the compensated spectra show a rise at large wave numbers, i.e., a different scaling regime emerges. (e, f) Log-log plot of energy spectra compensated by k^{ξ}, where the exponents ξ for each St and ϕ_m are given in the figure. In panels (c) and (e) the mass loading $\phi_m = 1$, while St = 0.67 in panels (d) and (f). The scaling exponents of energy spectra in the dust-dissipative range are obtained by doing a local slope analysis. The maximum standard error [35] on the local slope for each dataset is around ± 0.05.

with $\xi < 3.9$. This scaling range, which we henceforth call the *dust-dissipative* range, continues, in some cases, almost up to the dealiasing scale k_{max}. The scaling exponent ξ is *nonuniversal*—it depends on both the St and the mass-loading parameter ϕ_m. To demonstrate this we first compare the energy spectra for the case with no feedback (dashed black line) with three representative cases with feedback: $\phi_m = 1$ and three different values of St in Fig. 3(a). For $k < k_c$ all four spectra show the same scaling behavior. But for $k > k_c$, the spectrum without feedback ($\phi_m = 0$) falls off very sharply compared to the spectra with feedback. To explore the scaling behavior of the spectra in detail, in Fig. 3(b) we plot the same spectra compensated with $k^{3.9}$. For $k < k_c$ all the compensated spectra look horizontal, with fluctuations. In contrast, for

TABLE I. Scaling exponent $\xi = 5 - \gamma$ obtained from dominant balance of the viscous term ($\mathscr{D}$) and the contribution because of back-reaction from the dust particles to the gas ($\mathscr{R}$) [see Eq. (10)] for different values of the particle inertia (St) and the mass-loading parameter (ϕ_m). For comparison, in the last column, we provide the value of the same exponent ξ as obtained from the energy spectrum (Fig. 3). The maximum standard error in the estimation of the scaling exponents is around ± 0.05.

St	ϕ_m	$\xi = 5 - \gamma$	ξ (Fig. 3)
0.17	1.0	3.24	3.25
0.33	1.0	3.16	3.06
0.67	1.0	3.24	3.20
1.00	1.0	3.33	3.40
0.67	0.8	3.30	3.34
0.67	0.4	3.20	3.72

$k > k_c$ the compensated spectrum for the case with no feedback ($\phi_m = 0$) falls off sharply, indicating an exponential falloff, whereas the spectra with feedback grow with k, suggesting the emergence of a scaling regime with an exponent $\xi < 3.9$. Next we calculate ξ by a local slope analysis in the dust-dissipative range of the spectra with feedback. The values of ξ we obtain depend on St. Next, in Fig. 3(c) we plot the three spectra with feedback again, this time compensated with k^{ξ}. The range over which the spectra are horizontal shows the extent of the dust-dissipative range. Next, we do a similar analysis where we compare the case with no feedback again with three cases with feedback; but this time we hold $\mathrm{St} = 0.67$ fixed and consider three different values of ϕ_m. The corresponding figures are shown in the right column of Fig. 3. We systematically calculate the scaling exponent ξ for three values of St between 0.17 and 1.0 with $\phi_m = 1$ and for three values of ϕ_m between 0.4 and 1 with $\mathrm{St} = 0.67$. With St, we find that ξ first decreases, reaches its minimum value $\xi \sim 3$ for $\mathrm{St} = 0.33$ [see Figs. 3(d) and 3(e)], and then increases again. For a fixed $\mathrm{St} = 0.67$, ξ reduces monotonically as ϕ_m is increased [Figs. 3(b), 3(d), and 3(f)].

In Table I we list the scaling exponent ξ, obtained from the energy spectra, with its error estimate. It is not trivial to estimate the error in the measurement of ξ. We select the scaling range as the range over which the scaling exponent (obtained from local slope) of the energy spectra is within ± 0.1 of its mean value. We use the maximum standard error [35] of the local slope as a reasonable estimate of error. We have checked that, if we calculate the exponents ξ over half the dataset, the values obtained remain within the range of error. Note that the range of the scaling regime is not very large even in the best cases. Consequently, subleading terms in scaling behavior may contribute significantly [36]. The actual error in the determination of the scaling exponents is likely to be larger than the values we quote. In the next section, we calculate the exponent in another manner.

C. Enstrophy budget

To understand the scaling behavior we now study the scale-by-scale enstrophy budget equation:

$$\Pi(k) = \mathscr{D}(k) - \alpha\Omega(k) + \mathscr{F}(k) + \mathscr{R}(k). \tag{8}$$

Here

$$\Omega(k) \equiv \left\langle \sum_{m \leqslant k} \mid \omega_{\boldsymbol{m}} \mid^2 \right\rangle \tag{9a}$$

is the cumulative enstrophy up to wave number k;

$$\Pi(k) \equiv \left\langle \sum_{m \leqslant k} \omega_{\boldsymbol{m}} (\boldsymbol{u} \cdot \nabla \boldsymbol{\omega})_{-\boldsymbol{m}} \right\rangle \tag{9b}$$

is the enstrophy flux through a sphere of radius k in Fourier space due to the nonlinear term;

$$\mathscr{D}(k) \equiv -\nu \left\langle \sum_{m \leqslant k} m^2 \mid \omega_{\boldsymbol{m}} \mid^2 \right\rangle \tag{9c}$$

is the cumulative enstrophy dissipation rate; $-\alpha\Omega(k)$ is the contribution due to the Ekman friction;

$$\mathscr{F}(k) \equiv \left\langle \sum_{m \leqslant k} \omega_{\boldsymbol{m}} f_{-\boldsymbol{m}} \right\rangle \tag{9d}$$

is the cumulative enstrophy injected due to the Kolmogorov forcing; and

$$\mathscr{R}(k) \equiv \left\langle \sum_{m \leqslant k} \omega_{\boldsymbol{m}} (\nabla \times \boldsymbol{F}^{\mathrm{d}\to\mathrm{g}})_{-\boldsymbol{m}} \right\rangle \tag{9e}$$

is the contribution because of the back-reaction from the dust particles to the gas. In Fig. 4(a) we plot the enstrophy budget for the gas in the absence of particles ($\phi_m = 0$). Similar to earlier studies, we observe that at large scales enstrophy injected by external forcing is primarily balanced by the Ekman drag and the enstrophy flux $\Pi(k)$ decreases with increasing k [21].

We now show that the presence of dust particles dramatically alters the enstrophy budget in the range of wave numbers which belong to the dissipation range for the case with no feedback. In Fig. 4(b) we plot the cumulative contributions of all the terms in the budget for $\mathrm{St} = 0.67$ and $\phi_m = 1.0$. The dust particles inject enstrophy ($\mathscr{R}$) at large k which is then balanced by viscous dissipation $\mathscr{D}$. We find a negligible change in the shape of Π, $\mathscr{F}$, and the Ekman drag term in the inertial range. A closer look at $\mathscr{R}$ [Fig. 4(c)] reveals that it makes a net negative contribution to the budget till a wave number k_c after which it turns positive. Clearly, the particles extracts enstrophy from the flow at small k (large scale) but injects enstrophy at large k (small scale). Furthermore, for $k > k_c$ the two dominant terms that balance each other are the contribution because of the back-reaction from the dust particles to the gas $\mathscr{R}$ and the cumulative enstrophy dissipation due to viscosity $\mathscr{D}$, i.e., $\nu \sum_{m \leqslant k} m^4 E(m) \sim \mathscr{R}(k)$. Taking the derivative with respect to k, we get

$$E(k) \sim k^{-4} \frac{d\mathscr{R}(k)}{dk} \tag{10}$$

for $k > k_c$. In Figs. 5(a) and 5(b) we show that $\mathscr{R}(k) \sim k^{\gamma}$ for $k > k_c$. Using Eq. (10) and noting that $E(k) \sim k^{-\xi}$, we get $\xi = 5 - \gamma$. In Table I, we present the scaling exponents ξ evaluated using the dominant balance discussed above and those obtained from Fig. 3. Except for $\phi_m = 0.4$, the two different methods for estimating ξ are in reasonable agreement.

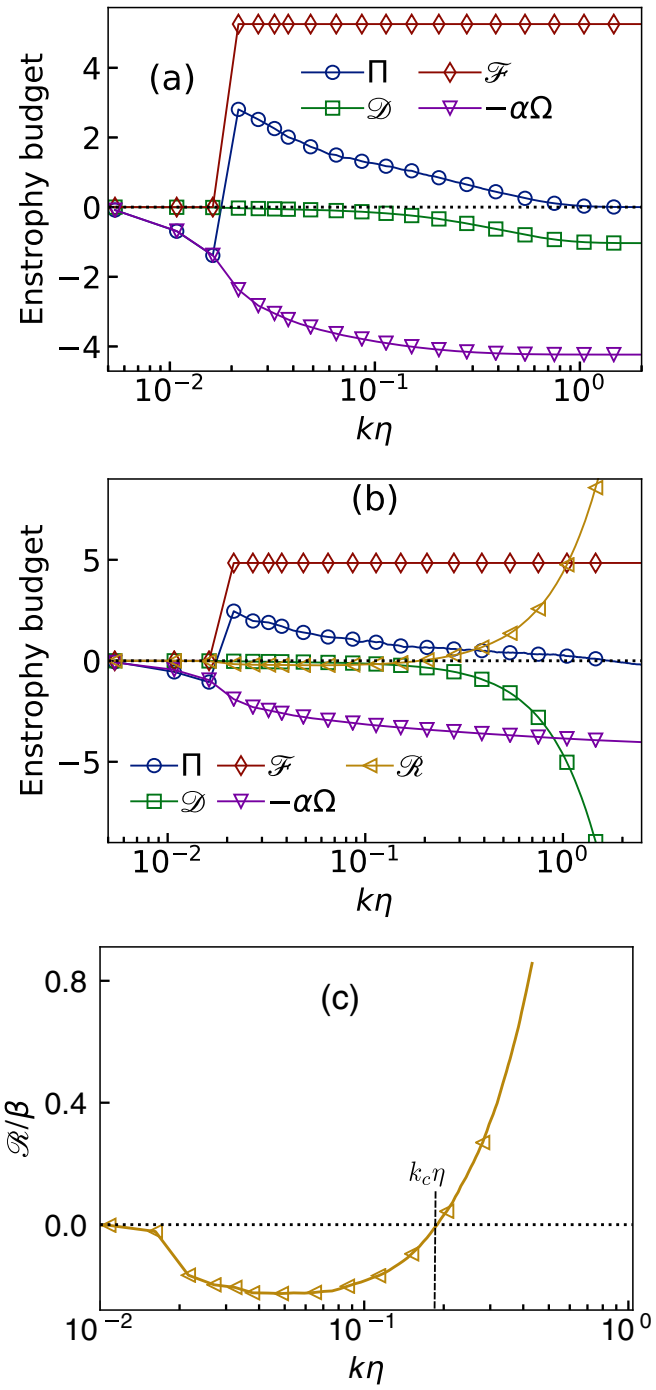

FIG. 4. Semilog (X axis in log scale) plot of scale-by-scale enstrophy budget for (a) $\phi_m = 0$ and (b) St $= 0.67$ and $\phi_m = 1$. (c) Semilog plot of $\mathscr{R}(k)$ zoomed for $k\eta \leqslant 0.4$. Note that $\mathscr{R}(k)$ changes sign from negative to positive at k_c. The ordinates of panels (a) and (b) are normalized by the enstrophy dissipation rate β.

Note that the range over which scalings are observed in Figs. 3 and 5 are slightly different.

We would like to point out that using arguments similar to the paragraph above, an equivalent prediction for the scaling of the energy spectrum can be also obtained from the steady-state spectral kinetic energy transfer equation [12,16]

$$T(k) = D(k) - \alpha E(k) + \mathcal{F}(k) + R(k), \qquad (11)$$

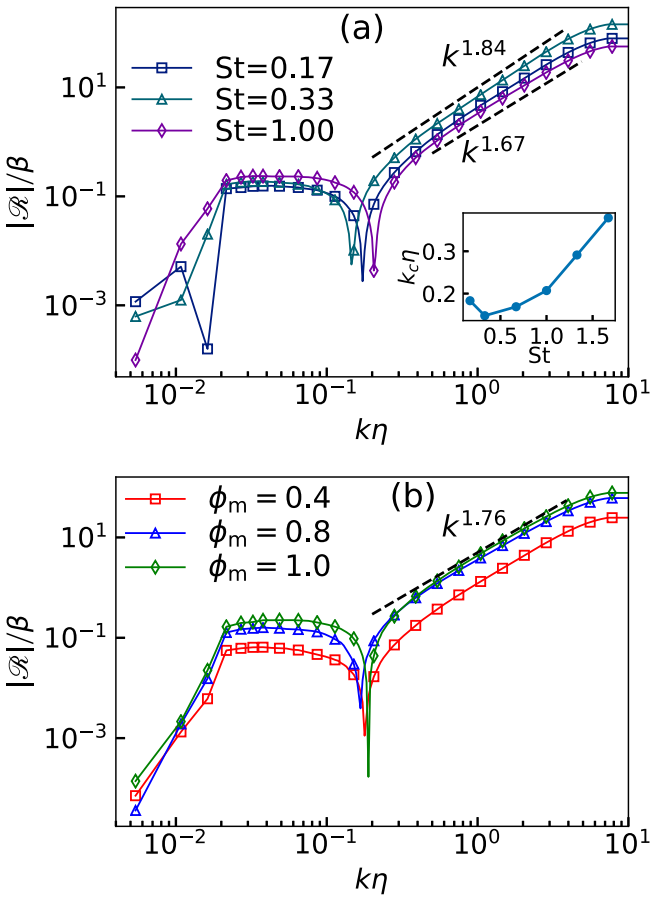

FIG. 5. Log-log plot of $\mathscr{R}(k)$ for (a) $\phi_m = 1$, different values of St, and (b) St $= 0.67$, different values of ϕ_m. (Inset) Linear plot of $k_c\eta$ [mode where $\mathscr{R}(k)$ changes sign] vs St. Dashed lines in both panels (a) and (b) show the scaling for $\mathscr{R}(k)$.

where

$$T(k) \equiv \left\langle \sum_{k-1/2\leqslant|m|<k+1/2} \boldsymbol{u_m}(\boldsymbol{u}\cdot\nabla\boldsymbol{u})_{-\boldsymbol{m}} \right\rangle \qquad (12)$$

is the transfer function;

$$R(k) \equiv \left\langle \sum_{k-1/2\leqslant|m|<k+1/2} \boldsymbol{u_m}(\boldsymbol{F}^{d\to g})_{-\boldsymbol{m}} \right\rangle \qquad (13)$$

is the contribution due to particle fluid coupling; $D(k) \equiv -\nu k^2 E(k)$ is the viscous dissipation rate; $-\alpha E(k)$ is the dissipation rate due to the Ekman drag;and $\mathcal{F}(k)$ is the energy injection rate due to the Kolmogorov forcing. Since $T(k)$ is negligible for $k > k_c$, the scaling exponent for the energy spectrum can also be obtained from the balance between $D(k)$ and $R(k)$.

IV. CONCLUSION

We use the Eulerian-Lagrangian formalism to study the effects of dust to gas coupling in two-dimensional turbulence. The dust is modeled as heavy inertial particles immersed in the gas. We solve gas equations on fixed Eulerian grids

by incorporating the forces [Eq. (3)] due to dust. The main problem with this technique is that to have a smooth Eulerian representation of the feedback, the number of particles per cell needs to be equal or greater than a certain threshold ($\approx$1) [37,38]. We choose N_p such that in the stationary state, i.e., after the dust has clustered, the above constraint is satisfied for almost all the St. Furthermore, we use higher-order weight function for extrapolation to ensure a smoother approximation of back-reaction on the fluid grids. We obtain reasonable scaling range for nearly all the St and ϕ_m.

The Eulerian-Lagrangian formalism has been extensively used to study how the interaction between dust and gas modifies three-dimensional turbulence. Here, we review some of them with an emphasis on energy spectra (see Refs. [37,39] and references therein for more details). References [40,41] studied the effects of dust in isotropic stationary turbulence using direct numerical simulations while similar studies in decaying turbulence were done by Refs. [42,43]. The key results of these studies are the following: (a) particles inject energy at large k and reduce it at small k, and (b) increasing mass loading leads to reduction of the total kinetic energy. However, the effects of changing the inertia of the dust particles (St) or the mass-loading parameter (ϕ_m) on the scaling of the energy spectra remained unclear as these simulations were done at small or moderate resolution. More recently, Refs. [44–46] introduced numerical schemes to model coupling between gas and dust. In brief, let us point out that the mollification function that we use spreads the back-reaction of a single particle up to 16 neighboring grid points and is similar to the Gaussian kernel used in Refs. [44,45]. We avoid additional computational cost by not implementing the additional diffusion filter of Ref. [44] or the exact regularization protocol of Ref. [45]. One major advantage of the method of Ref. [45] is that the number of particles need not be comparable to the number of grid cells for smooth feedback. Unfortunately, the method is computationally expensive and not easily parallelizable on distributed-memory machines. By studying dust-laden homogeneous shear turbulent flow using this technique, Gualtieri *et al.* [15] reported a scaling exponent of -4 in a gas kinetic energy spectrum [for St $= 1$ and $\phi_m = (0.4, 0.8)$]. They argued that this scaling appears due to the balance of viscous forces with the back-reaction from dust. In Ref. [15], the critical wave number beyond which this scaling was observed was found to be $k_c\eta \geqslant 1$, whereas our two-dimensional study shows $k_c\eta \sim 0.2$. Clearly, the crucial problem with our and similar studies is that there is, as yet, no well-established algorithm to numerically calculate the feedback in DNS.

For good reasons, the most important one being difficulties in experimental realization, turbulence in flows of dust and gas has been rarely studied in two dimensions. Using a Eulerian description of dust, Bec. *et al.* [31] found a scaling exponent of -2 in the gas energy spectra, which emerges due to the balance of the nonlinear transfer against the feedback, for St $\ll 1$ and ϕ_m between 0.1 and 0.4. To numerically smooth the caustics that invariably develops in such a computation a synthetic hyperviscous term was added in the Eulerian description. The Ekman drag coefficient was chosen such that the pure gas spectra (without dust coupling) scale with an exponent of -3.3. Notably, the scaling here starts at much smaller k compared to what we find.

Our main results can be summarized as follows.

(a) The presence of dust-gas coupling decreases clustering of dust particles.

(b) A different scaling regime emerges in the kinetic energy spectrum.

(c) The scale-by-scale enstrophy budget suggests that this scaling is because of gas viscosity dissipating the enstrophy injected by dust at those scales.

(d) Dust has a net negative contribution to the budget till a wave number k_c and injects enstrophy at higher Fourier modes.

(e) Because the form of dust-gas coupling term varies with both ϕ_m and more importantly St, the scaling exponent is nonuniversal and a function of both.

Even in two dimensions, where we have been able to do large-scale simulations for a long enough time, the appearance of the emerging scaling regime is not always prominent. We cannot rule out the possibility that there may be no scaling range at all, but we can and do conclude that the scaling of energy spectra is *nonuniversal*.

It is quite difficult to perform a DNS of similar resolution, with feedback from particles, in three dimensions. So it is unlikely that in the near future we shall observer clear scaling behavior in analogous cases in three dimensions, but based on our results we speculate that the same *nonuniversal* nature of spectra will be true in three dimensions too.

ACKNOWLEDGMENTS

We thank Paolo Gualtieri for useful discussions. D.M. acknowledges financial support from the grant Bottlenecks for particle growth in turbulent aerosols from the Knut and Alice Wallenberg Foundation (diary number KAW 2014.0048) and from the Swedish Research Council under Grants No. 638-2013-9243 and No. 2016-05225.

[1] P. J. Armitage, *Astrophysics of Planet Formation* (Cambridge University, Cambridge, England, 2010).

[2] H. Pruppacher and J. Klett, *Microphysics of Clouds and Precipitation* (Springer, New York, 2010), Vol. 18.

[3] J. F. Kok, E. J. Parteli, T. I. Michaels, and D. B. Karam, Rep. Prog. Phys. **75**, 106901 (2012).

[4] L. I. Zaichik, V. M. Alipchenkov, and E. G. Sinaiski, *Particles in Turbulent Flows* (Wiley-VCH, Berlin, 2008).

[5] F. Toschi and E. Bodenschatz, Annu. Rev. Fluid Mech. **41**, 375 (2009).

[6] A. Pumir and M. Wilkinson, Annu. Rev. Condens. Matter Phys. **7**, 141 (2016).

[7] K. Gustavsson and B. Mehlig, Adv. Phys. **65**, 1 (2016).

[8] A. N. Youdin and J. Goodman, Astrophys. J. **620**, 459 (2005).

[9] A. Johansen and A. Youdin, Astrophys. J. **662**, 627 (2007).

[10] U. Frisch, *Turbulence the Legacy of A. N. Kolmogorov* (Cambridge University, Cambridge, England, 1996).

[11] S. Pope, *Turbulent Flows* (Cambridge University, Cambridge, England, 2000).

[12] P. Davidson, *Turbulence* (Oxford University, New York, 2004).

[13] A. Kolmogorov, Dokl. Acad. Nauk USSR **30**, 9 (1941).
[14] Experiments and recent numerical simulations have demonstrated that the Kolmogorov picture is not complete, but must include corrections due to intermittency. The intermittency corrections to the energy spectrum are small and are ignored in this paper.
[15] P. Gualtieri, F. Battista, and C. M. Casciola, Phys. Rev. Fluids **2**, 034304 (2017).
[16] M. Lesieur, *Turbulence in Fluids*, Fluid Mechanics and Its Applications (Springer, Dordrecht, The Netherlands, 1997), Vol. 40.
[17] R. Fjørtoft, Tellus **5**, 226 (1953).
[18] R. Kraichnan, Phys. Fluids **10**, 1417 (1967).
[19] G. K. Batchelor, Phys. Fluids Suppl. II **12**, 233 (1969).
[20] C. Leith, Phys. Fluids **11**, 671 (1968).
[21] G. Boffetta and R. E. Ecke, Annu. Rev. Fluid Mech. **44**, 427 (2012).
[22] R. Kraichnan and D. Montgomery, Rep. Prog. Phys. **43**, 547 (1980).
[23] K. Nam, E. Ott, T. M. Antonsen, and P. N. Guzdar, Phys. Rev. Lett. **84**, 5134 (2000).
[24] G. Boffetta, A. Cenedese, S. Espa, and S. Musacchio, Europhys. Lett. **71**, 590 (2005).
[25] M. K. Verma, Europhys. Lett. **98**, 14003 (2012).
[26] C. Canuto, M. Hussaini, A. Quarteroni, and T. Zang, *Spectral Methods in Fluid Dynamics* (Spinger-Verlag, Berlin, 1988).
[27] P. Perlekar, S. S. Ray, D. Mitra, and R. Pandit, Phys. Rev. Lett. **106**, 054501 (2011).
[28] W. Press, B. Flannery, S. Teukolsky, and W. Vetterling, *Numerical Recipes in Fortran* (Cambridge University, Cambridge, England, 1992).
[29] C. S. Peskin, Acta Numerica **11**, 479 (2002).
[30] R. A. Shaw, Annu. Rev. Fluid Mech. **35**, 183 (2003).
[31] J. Bec, L. François, and M. Stefano, arXiv:1702.06773v1.
[32] P. Grassberger and I. Procaccia, Phys. Rev. Lett. **50**, 346 (1983).
[33] J. Bec, L. Biferale, M. Cencini, A. Lanotte, S. Musacchio, and F. Toschi, Phys. Rev. Lett. **98**, 084502 (2007).
[34] P. Gualtieri, F. Picano, G. Sardina, and C. M. Casciola, J. Phys.: Conf. Ser. **333**, 012007 (2011).
[35] I. Hughes and T. Hase, *Measurements and Their Uncertainties: A Practical Guide to Modern Error Analysis* (Oxford University, Oxford, 2010).
[36] D. Mitra, J. Bec, R. Pandit, and U. Frisch, Phys. Rev. Lett. **94**, 194501 (2005).
[37] S. Balachandar and J. K. Eaton, Annu. Rev. Fluid Mech. **42**, 111 (2010).
[38] P. Gualtieri, F. Picano, G. Sardina, and C. M. Casciola, J. Fluid Mech. **715**, 134 (2013).
[39] C. Poelma and G. Ooms, Appl. Mech. Rev. **59**, 78 (2006).
[40] K. D. Squires and J. K. Eaton, Phys. Fluids A **2**, 1191 (1990).
[41] M. Boivin, O. Simonin, and K. D. Squires, J. Fluid Mech. **375**, 235 (1998).
[42] A. Ferrante and S. Elghobashi, Phys. Fluids **15**, 315 (2003).
[43] S. Sundaram and L. R. Collins, J. Fluid Mech. **379**, 105 (1999).
[44] J. Capecelatro and O. Desjardins, J. Comput. Phys. **238**, 1 (2013).
[45] P. Gualtieri, F. Picano, G. Sardina, and C. M. Casciola, J. Fluid Mech. **773**, 520 (2015).
[46] G. Sardina, K. Jareteg, H. Ström, and S. Sasic, Chem. Eng. Sci. **201**, 58 (2019).